Computing strain-dependent energy transfer from quantum dots to 2D materials

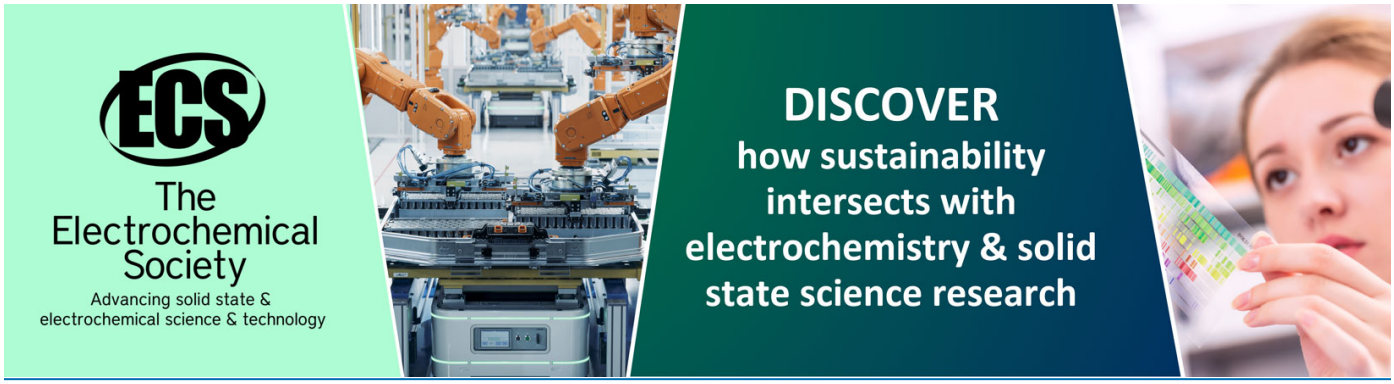

NANO FUTURES

PAPER

Computing strain-dependent energy transfer from quantum dots to 2D materials

Esra Şimşek and Burak Aslan*

Department of Physics, Bogazici University, Rumeli Hisarı, Nispetiye Cd No:7, Kuzey Kampüs Kare Blok, Bebek, Istanbul 34342, Turkey
* Author to whom any correspondence should be addressed.

E-mail: aslan@boun.edu.tr

Keywords: WS_2, graphene, monolayers, 2D materials, quantum dots, strain, non-radiative energy transfer

Supplementary material for this article is available online

OPEN ACCESS

RECEIVED
30 March 2023

REVISED
15 May 2023

ACCEPTED FOR PUBLICATION
12 June 2023

PUBLISHED
27 June 2023

Abstract

Near-field interaction between the monolayers of two-dimensional (2D) materials has been recently investigated. Another branch under investigation has been the interaction between 2D materials and zero-dimensional (0D) nanostructures including quantum dots (QDs) and metal nanoparticles. In this work, we take one more step to engineering the interaction between those systems. We probe the effect of mechanical strain on the non-radiative energy transfer (NRET) rate from a 0D material, ZnCdSe/ZnSe QD, to a 2D material, monolayer (1L) WS_2. It is known that the mechanical strain causes large shifts to the exciton energies in 1L WS_2. As a result, our calculations show that strain can tune the NRET rate by engineering the overlap between the emission spectrum of ZnCdSe/ZnSe QD and the exciton resonances of 1L WS_2.

1. Introduction

1.1. Non-radiative energy transfer

Non-radiative energy transfer (NRET) is the process of exciton transfer from a donor to an acceptor without the emission of photons. At short distances, NRET is the dominant decay channel due to coupling from the near field [1, 2] and it is an integral part of solar cells [3], photosynthesis [4], and quantum-dot-based light-emitting diodes [5]. NRET rate depends on certain factors such as spectral overlap between the acceptor's absorption and donor's emission, screening of the electric field [6], the distance between the donor and acceptor, and the thickness of the acceptor [7]. NRET rate also depends on the dimensions of the donor and acceptor media; in this work, we inspect that from a zero-dimensional (0D) donor to a 2D acceptor.

1.2. Techniques for tuning and choice of strain

Numerous tools have been used to alter the dielectric properties of two-dimensional (2D) materials in the last decade. Those include magnetic field [8], electrostatic gating [9, 10], changing the dielectric environment (substrate and superstrate) [11–13], and strain tuning [14–20]. 2D materials can also be integrated with special structures and materials such as nanocavities, photonic crystals, and metamaterials to tune the light–matter interaction and even enable normally forbidden optical transitions [21–23]. As the 2D materials are fairly strong, they can endure much larger strains than their bulk counterparts [24]. Strain engineering has become a topic of interest in the literature as the optoelectronic properties of transition metal dichalcogenides (TMDCs) strongly depend on strain [17, 25–31]. Studies have shown that strain tuning has some advantages over other methods; it is dynamic, reversible, and can cause larger changes to 2D materials as compared to other techniques. Strain tuning also has a fairly small effect on the exciton binding energies and the relative energy separations between the excitons as compared to the other techniques aforementioned [17]. Therefore, applying strain to the energy acceptor is an effective way to control the NRET rate since it significantly influences the spectral overlap of the acceptor and the donor media [17].

On that account, we compute the strain-dependent dielectric function of a 2D material. We calculate the NRET rate as a function of strain and show that it can be substantially tuned by purely mechanical means.

Our results exemplify the use of mechanical strain as a means of shedding light on the interaction between low-dimensional material systems.

1.3. Choice of materials

We choose monolayer (1L) WS_2 as the acceptor. We choose it among the commonly used semiconducting group-6 TMDCs (WS_2, WSe_2, MoS_2, $MoSe_2$, and $MoTe_2$); as it has the smallest *A* exciton linewidth at room temperature, which is also the least sensitive to strain [2, 17, 19, 32]. As a comparison, we investigate the NRET rate from QDs to 1L graphene. As graphene does not exhibit resonances in the emission range of the QD, the spectral dependence of the NRET rate is weaker. Furthermore, the strain does not cause significant changes to the dielectric function of graphene, making it a reference material for the strain-tuned NRET study in this work.

We choose the emitters as core–shell QDs with spherical symmetry because they possess high PL yield and it would be easy to observe any decrease in their PL. Furthermore, their band-edge excitons exhibit a long lifetime before recombination that leaves enough time for the excitons to transfer non-radiatively. Thus, it is intriguing to study the NRET between a QD and a 2D material as its substrate. As their band gaps can be engineered [33, 34], we pick one with a band gap close to that of the 2D material. We use ZnCdSe/ZnSe QDs [35–37].

1.4. Structure

In this work, we consider QDs placed on a 2D material without any spacing material, with air above and below the 0D-2D system. We assume that QDs are excited only, and there is no emission of photons from the 2D material.

2. Methods

2.1. Calculation of NRET

To calculate the NRET rate from the QD to the 2D material, we use the continuum model derived by Gordon and Gartstein [38]. We do not apply the Förster resonance energy transfer model as it treats the thin film acceptor as a combination of non-interacting point-like dipoles which underestimates the dielectric screening effect [39].

In the Gordon–Gartstein model, the energy donor acts like a classical dipole and exhibits spontaneous decay with a rate of $\Gamma_o = \frac{4k^3|\vec{p}|^2}{3\hbar}$ in vacuum, where k is the wave number and $|\vec{p}|$ is the (effective) transition dipole moment. As the QDs possess spherical symmetry and their size is much smaller than the wavelength of light, they can be treated as dipoles centered at the core of the QDs for spontaneous emission purposes [40]. In the electrostatic limit ($c \to \infty$), Γ_{QD-2D} is the NRET rate from a point dipole to an anisotropic 2D acceptor which can be expressed as follows:

$$\frac{\Gamma_{QD-2D}}{\Gamma_0} = \frac{2(\hbar c)^3}{3(Ed)^3} \times \mathrm{Im}\left[\int_0^\infty \mathrm{d}\rho\rho^2 \mathrm{e}^{-2\rho} \times \frac{\left(\beta^2-1\right)\left(1-\mathrm{e}^{-2\rho\delta t/d}\right)}{(\beta+1)^2-(\beta-1)^2\mathrm{e}^{-2\rho\delta t/d}}\right] \tag{1}$$

where $d = 3.32$ nm, the radius of the QDs, is taken as the distance between the acceptor and the donor [41], t is the thickness of the thin film acceptor (0.62 nm per WS_2 layer [42], 0.33 nm per graphene layer [43]), $\beta = \sqrt{\varepsilon_\parallel \varepsilon_\perp}$ (effective permittivity of the acceptor) and $\delta = \sqrt{\varepsilon_\parallel/\varepsilon_\perp}$ (dielectric anisotropy of the acceptor), where $\varepsilon_\parallel$ is the in-plane and $\varepsilon_\perp$ is the out-of-plane dielectric function of the acceptor. We treat the WS_2 layer as an infinitely large homogeneous slab with a finite thickness of t. As mentioned in section 1.3, we treat the QDs as finite-size balls with spherical symmetry.

2.2. Dielectric function of WS_2

We need the in-plane and out-of-plane dielectric function of 1L WS_2 for the NRET calculations. We take $\varepsilon_\perp$ of 1L WS_2 to be constant ($\sim$7) in the spectral region of interest (1.5–3.2 eV) [44]. We also take the energy-dependent $\varepsilon_\parallel$ of 1L WS_2 ($\varepsilon_\parallel^{1L\ WS_2}$) from the literature [45]. In the energy range of interest, $\varepsilon_\parallel^{1L\ WS_2}$ exhibits 4 features (*A*, *B*, *C*, *D* excitons/resonances). We model $\varepsilon_\parallel^{1L\ WS_2}$ as the sum of 4 Lorentz oscillators, corresponding to 1 oscillator for each of those features as expressed in equation (2),

$$\varepsilon_\parallel(E) = \varepsilon_b + \sum_{m=1}^{4} \frac{f_m}{E_m^2 - E^2 - \mathrm{i}E\gamma_m}. \tag{2}$$

Here E is the photon energy, f_m is the oscillator strength, γ_m is the linewidth, and E_m is the resonance energy of the mth oscillator, ε_b is the background dielectric constant representing the contribution of the

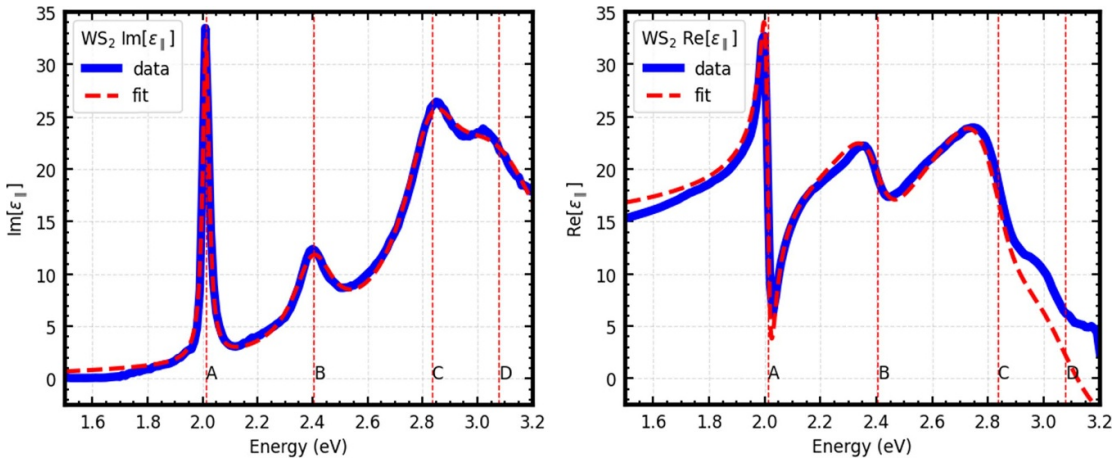

Figure 1. Experimentally obtained data (solid curves) [45] and fit (dashed curves) of the imaginary (left) and real (right) part of the dielectric function of 1L WS_2. Dashed vertical lines indicate the peak energy of the *A*, *B*, *C*, *D* features. Reprinted figure with permission from [45], Copyright (2023) by the American Physical Society.

higher energy resonances not included in our model. We first fit the imaginary part of the experimentally obtained dielectric function to the superposition of 4 Lorentzian oscillators. We calculate the real part of the dielectric function using the results of the fit to the imaginary part. We optimize the calculated real part by adjusting ε_b and make sure that it is in good agreement with the experimentally obtained $\varepsilon_{\|}$ [45]. We compute the dielectric function of 1L WS_2 from equation (2) using the fit results. Figure 1 shows the experimentally obtained values of $\varepsilon_{\|}^{1L\,WS_2}$ and the results of the fits. As we do not take into account the contributions from features outside the range of the fit, it is impossible to fully capture the experimental results. As a result, there is a large mismatch beyond the *C* feature energy in the real part of $\varepsilon_{\|}$. As the NRET will occur around the *A* exciton energy, the mismatch beyond the *C* feature is insignificant for our calculations.

3. Results and discussion

3.1. Strain-dependent dielectric function of WS_2

Strain affects the band structure of 2D materials resulting in a change in their dielectric function [25–31]. Therefore, to compute equation (1) as a function of strain, we need to obtain the dielectric function of the host material as a function of strain. To do so, we take the Lorentzian components mentioned above into account. For that, we make use of the experimentally available data on the effect of strain on the resonances of 1L WS_2. We refer to uniaxial strain in this work unless otherwise specified. *A* exciton shifts by −45.2 meV/% strain, *B* exciton shifts by −35.7 meV/% strain, and *C* feature shifts by −20.7 meV/% strain in 1L WS_2 [17, 19]. In our calculations, we ignore the shift of the *D* feature due to the lack of data in the literature. As the *D* feature is far from the QD emission range, it does not affect the calculations. We ignore the effect of strain on the oscillator strengths and the line widths; as the former is small and the latter is relatively small for WS_2 [2, 17, 46]. We also assume that the aforementioned statements are valid over the range of strain values reported in this study. We compute the strain-dependent Lorentzian lineshapes as described above, yielding the strain-dependent dielectric function. Figure 2 shows the strain-dependent real and imaginary parts of $\varepsilon_{\|}^{1L\,WS_2}$. With that, we calculate the rate Γ/Γ_0 as a function of strain in the energy range of 1.5–3.2 eV.

3.2. Computation of NRET rate

We need to consider the emission spectrum of the QD samples. As QDs are mostly found in aggregates, rather than isolated particles, the inhomogeneity in the collection result in PL spectra with Gaussian lineshape. For that reason, we fit the PL of such a sample of ZnCdSe/ZnSe QDs to a Gaussian line shape and obtain a peak at 613.2 nm [47].

We apply the classical model to calculate the NRET rate between the QD and the 1L WS_2 [6, 7, 10]. Figure 3 shows the NRET rate (normalized by the dipole emission to vacuum), $\frac{\Gamma_{QD-2D}}{\Gamma_0}$, as a function of energy for selected strain levels. As the thickness of the material is very small, the screening effect (governed by the imaginary part of $\varepsilon_{\|}$) is not dominant. As a result, the NRET rates in figure 3 resemble the imaginary part of the $\varepsilon_{\|}$ of WS_2. Figure 3 also shows the product of QD's normalized PL and NRET rate under strain as

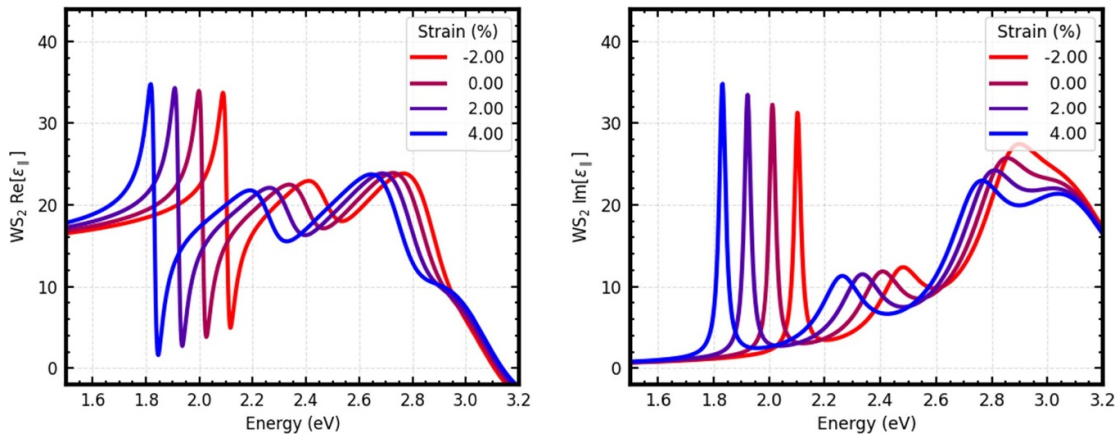

Figure 2. Calculated strain-dependent real (left) and imaginary (right) part of the in-plane dielectric function ($\varepsilon_{\parallel}$) of 1L WS_2.

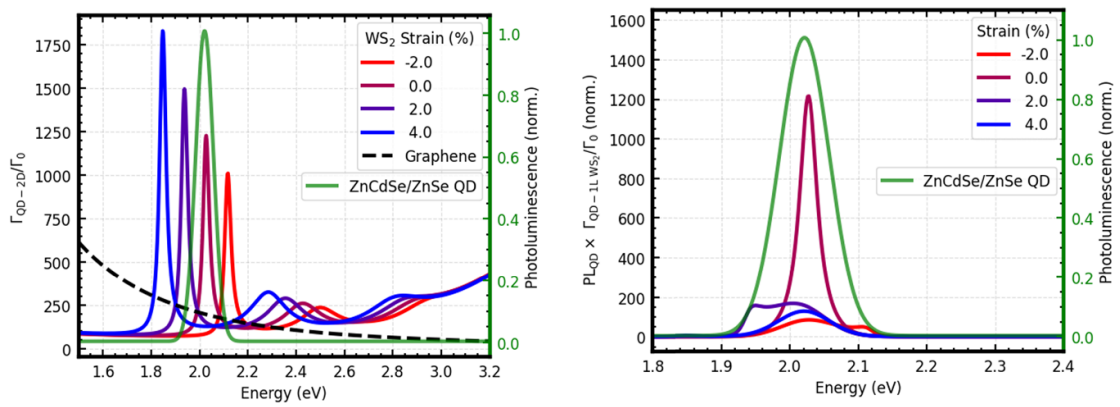

Figure 3. (Left): Calculated NRET rate from ZnCdSe/ZnSe QD to monolayer WS_2 for selected strain levels and to monolayer graphene (normalized by dipole emission in vacuum), (Right) Normalized PL spectrum of QD and PL multiplied by the calculated rate in (left).

a function of energy, $\mathrm{PL_{QD}} \times \frac{\Gamma_{\mathrm{QD-1L\,WS_2}}}{\Gamma_0}$. The rate is dominated by the overlap between the *A* exciton peak in $\mathrm{Im}[\varepsilon_{\parallel}]$ of 1L WS_2 and the QD PL spectrum which is strongly dependent on the strain applied.

3.3. Total NRET as a function of strain

To obtain the NRET rate for this specific emission spectrum, we integrate the product of the PL spectrum and Γ/Γ_0 and normalize by the total emission of the QD:

$$\mathrm{Total}\,(s) = \frac{\int_{1.5\ \mathrm{eV}}^{3.2\ \mathrm{eV}} \Gamma/\Gamma_0\,(s,E) \times \mathrm{PL_{QD}}\,(E)\,\mathrm{d}E}{\int_{1.5eV}^{3.2eV} \mathrm{PL_{QD}}\,(E)\,\mathrm{d}E}. \tag{3}$$

Here, *s* is strain, *E* is energy, $\mathrm{PL_{QD}}$ is the PL emission of the QD. We plot this strain-dependent function and found the strain-dependent Γ/Γ_0 rate between the QD and 1L WS_2 theoretically. In figure 4, we plot the total NRET rate between a ZnCdSe/ZnSe quantum dot and 1L WS_2 as a function of uniaxial strain. We see that the NRET rate is nearly maximized at around 0% strain due to the overlap between the emission spectrum of the QD and the absorption due to the *A* exciton in unstrained WS_2. At larger strain levels, the *A* exciton is significantly redshifted so that the NRET rate is highly reduced to a minimum at around 4% strain. For strain levels larger than about 4%, the *B* exciton starts overlapping with the QD peak and the NRET rate starts increasing again. The ratio of the maximum to minimum NRET rate is around 4 which can be achieved with a relatively small range of 4% uniaxial strain. Biaxial strain induces a redshift to the *A* exciton in 1L WS_2 approximately twice that of the uniaxial strain [48]. Therefore, a 2% biaxial strain, which was demonstrated on suspended MoS_2 [20], would show the same tuning effect.

It would be good to consider the validity of our assumption in 1.3 that there is no emission from the 2D material. That assumption would require the quantum efficiency of the 2D material to be much smaller than that of the QD on the 2D material. As shown in the literature, QDs placed on 2D materials will exhibit a

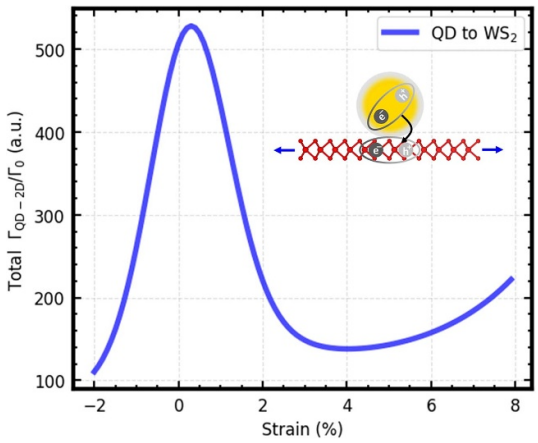

Figure 4. Total NRET rate between a 0D, ZnCdSe/ZnSe quantum dot, and a 2D material, 1L WS_2, as a function of strain. The inset is an illustration of the strain-dependent transfer of an exciton created in the quantum dot to the 2D material.

smaller PL yield than those placed on a non-dissipative substrate (such as quartz) due to the very NRET effect [6]. However, 2D materials have quantum yields of less than 1% [49]. As thicker 2D layers have much a smaller quantum yield than monolayers, in the case the PL of the two systems are indistinguishable, thicker 2D layers will satisfy that requirement much more easily [50].

4. Conclusion

In conclusion, our calculations show that by utilizing strain engineering, it is possible to tune the NRET interaction between a 0D and a 2D material, 1L WS_2. The ground state *A* exciton in 1L WS_2 has alarge binding energy and small spectral line width at room temperature. As a result, a broad range in the dielectric function of the material is mainly influenced by the ground state *A* exciton only. That way the *A* exciton can be shifted over a large spectral range to tune any interaction governed by the dielectric function in 1L WS_2. Including the sensitivity to mechanical strain, all these factors enable strong tuning of NRET via strain. Our calculations can be repeated for other 2D materials and various thicknesses. The results can be tested with experiments and utilized for applications such as strain detection sensors, strain-tuned near-field phenomena, and strong coupling [51].

Data availability statement

All data that support the findings of this study are available online.

Acknowledgments

This Project has been supported by Boğaziçi Üniversitesi Bilimsel Araştırma Projeleri (21B03SUP4) and TÜBİTAK (Project No: 118C325). TÜBİTAK's support does not imply any endorsement of the scientific content of this work.

ORCID iD

Burak Aslan https://orcid.org/0000-0002-0925-3026

References

[1] Liu K C and George T F 1985 Spontaneous emission by two atoms with different resonance frequencies near a metal surface *Phys. Rev.* B **32** 3622
[2] Niehues I *et al* 2018 Strain control of exciton-phonon coupling in atomically thin semiconductors *Nano Lett.* **18** 1751
[3] Hardin B E, Snaith H J and McGehee M D 2012 The renaissance of dye-sensitized solar cells *Nat. Photon.* **6** 162
[4] Scholes G D, Fleming G R, Olaya-Castro A and van Grondelle R 2011 Lessons from nature about solar light harvesting *Nat. Chem.* **3** 763
[5] Shirasaki Y, Supran G J, Bawendi M G and Bulović V 2013 Emergence of colloidal quantum-dot light-emitting technologies *Nat. Photon.* **7** 13
[6] Raja A *et al* 2016 Energy transfer from quantum dots to graphene and MoS_2: the role of absorption and screening in two-dimensional materials *Nano Lett.* **16** 2328

[7] Prins F, Goodman A J and Tisdale W A 2014 Reduced dielectric screening and enhanced energy transfer in single- and few-layer MoS_2 *Nano Lett.* **14** 6087
[8] Stier A V, Wilson N P, Clark G, Xu X and Crooker S A 2016 Probing the influence of dielectric environment on excitons in monolayer WSe_2: insight from high magnetic fields *Nano Lett.* **16** 7054
[9] Chernikov A, van der Zande A M, Hill H M, Rigosi A F, Velauthapillai A, Hone J and Heinz T F 2015 Electrical tuning of exciton binding energies in monolayer WS_2 *Phys. Rev. Lett.* **115** 126802
[10] Prasai D *et al* 2015 Electrical control of near-field energy transfer between quantum dots and two-dimensional semiconductors *Nano Lett.* **15** 4374
[11] Waldecker L *et al* 2019 Rigid band shifts in two-dimensional semiconductors through external dielectric screening *Phys. Rev. Lett.* **123** 206403
[12] Borghardt S, Tu J-S, Winkler F, Schubert J, Zander W, Leosson K and Kardynał B E 2017 Engineering of optical and electronic band gaps in transition metal dichalcogenide monolayers through external dielectric screening *Phys. Rev. Mater.* **1** 54001
[13] Raja A *et al* 2017 Coulomb engineering of the bandgap and excitons in two-dimensional materials *Nat. Commun.* **8** 15251
[14] Schmidt R, Niehues I, Schneider R, Drüppel M, Deilmann T, Rohlfing M, de Vasconcellos S M, Castellanos-Gomez A and Bratschitsch R 2016 Reversible uniaxial strain tuning in atomically thin WSe_2 *2D Mater.* **3** 2
[15] Aslan B, Yule C, Yu Y, Lee Y J, Heinz T F, Cao L and Brongersma M L 2022 Excitons in strained and suspended monolayer WSe_2 *2D Mater.* **9** 015002
[16] Yang S X, Chen Y J and Jiang C B 2021 Strain engineering of two-dimensional materials: methods, properties, and applications *Infomat* **3** 397
[17] Aslan B, Deng M and Heinz T F 2018 Strain tuning of excitons in monolayer WSe_2 *Phys. Rev.* B **98** 115308
[18] Deng S, Sumant A V and Berry V 2018 Strain engineering in two-dimensional nanomaterials beyond graphene *Nano Today* **22** 14
[19] Aslan B, Deng M, Brongersma M L and Heinz T F 2020 Strained bilayer WSe_2 with reduced exciton-phonon coupling *Phys. Rev.* B **101** 115305
[20] Lloyd D, Liu X H, Christopher J W, Cantley L, Wadehra A, Kim B L, Goldberg B B, Swan A K and Bunch J S 2016 Band gap engineering with ultralarge biaxial strains in suspended monolayer MoS_2 *Nano Lett.* **16** 5836
[21] Ma X, Youngblood N, Liu X, Cheng Y, Cunha P, Kudtarkar K, Wang X and Lan S 2021 Engineering photonic environments for two-dimensional materials *Nanophotonics* **10** 1031
[22] Ma X *et al* 2022 Coherent momentum control of forbidden excitons *Nat. Commun.* **13** 6916
[23] Rivera N and Kaminer I 2020 Light–matter interactions with photonic quasiparticles *Nat. Rev. Phys.* **2** 538
[24] Bertolazzi S, Brivio J and Kis A 2011 Stretching and breaking of ultrathin MoS_2 *ACS Nano* **5** 9703
[25] Yun W S, Han S W, Hong S C, Kim I G and Lee J D 2012 Thickness and strain effects on electronic structures of transition metal dichalcogenides: 2H-*MX2* Semiconductors (M = Mo, W; X = S, Se, Te) *Phys. Rev.* B **85** 33305
[26] Yan Y, Ding S, Wu X, Zhu J, Feng D, Yang X and Li F 2020 Tuning the physical properties of ultrathin transition-metal dichalcogenides via strain engineering *RSC Adv.* **10** 39455
[27] Maniadaki A E, Kopidakis G and Remediakis I N 2016 Strain engineering of electronic properties of transition metal dichalcogenide monolayers *Solid State Commun.* **227** 33
[28] Dai Z, Liu L and Zhang Z 2019 Strain engineering of 2D materials: issues and opportunities at the interface *Adv. Mater.* **31** 1805417
[29] Naumis G G, Barraza-Lopez S, Oliva-Leyva M and Terrones H 2017 Electronic and optical properties of strained graphene and other strained 2D materials: a review *Rep. Prog. Phys.* **80** 96501
[30] Song W and Yang L 2017 Quasiparticle band gaps and optical spectra of strained monolayer transition-metal dichalcogenides *Phys. Rev.* B **96** 235441
[31] Zollner K, Junior P E F and Fabian J 2019 Strain-tunable orbital, spin-orbit, and optical properties of monolayer transition-metal dichalcogenides *Phys. Rev.* B **100** 195126
[32] Cadiz F *et al* 2017 Excitonic linewidth approaching the homogeneous limit in MoS_2-based van der Waals heterostructures *Phys. Rev.* X **7** 21026
[33] Karel Čapek R, Moreels I, Lambert K, De Muynck D, Zhao Q, Van Tomme A, Vanhaecke F and Hens Z 2010 Optical properties of zincblende cadmium selenide quantum dots *J. Phys. Chem.* C **114** 6371
[34] Baskoutas S and Terzis A F 2006 Size-dependent band gap of colloidal quantum dots *J. Appl. Phys.* **99** 013708
[35] Onal A *et al* 2022 High-performance white light-emitting diodes over 150 Lm/W using near-unity-emitting quantum dots in a liquid matrix *ACS Photon.* **9** 1304
[36] Li Z, Chen F, Wang L, Shen H, Guo L, Kuang Y, Wang H, Li N and Li L S 2018 Synthesis and evaluation of ideal core/shell quantum dots with precisely controlled shell growth: nonblinking, single photoluminescence decay channel, and suppressed FRET *Chem. Mater.* **30** 3668
[37] Zhang T, Zhang X, Yang P, Bai J, Chang C, Jin X, Zhao F, Huang Y and Li F 2019 Bright alloy CdZnSe/ZnSe QDs with nonquenching photoluminescence at high temperature and their application to light-emitting diodes *J. Nanomater.* **2019** 9257018
[38] Gordon J M and Gartstein Y N 2013 Dielectric polarization, anisotropy and nonradiative energy transfer into nanometre-scale thin semiconducting films *J. Phys.: Condens. Matter* **25** 425302
[39] Swathi R S and Sebastian K L 2009 Long range resonance energy transfer from a dye molecule to graphene has (Distance)-4 dependence *J. Chem. Phys.* **130** 086101
[40] Kristensen P T, Mortensen J E, Lodahl P and Stobbe S 2013 Shell theorem for spontaneous emission *Phys. Rev.* B **88** 205308
[41] Dabbousi B O, Rodriguez-Viejo J, Mikulec F V, Heine J R, Mattoussi H, Ober R, Jensen K F and Bawendi M G 1997 (CdSe)ZnS core-shell quantum dots: synthesis and characterization of a size series of highly luminescent nanocrystallites *J. Phys. Chem.* B **101** 9463
[42] Wilson J A and Yoffe A D 1969 The transition metal dichalcogenides discussion and interpretation of the observed optical, electrical and structural properties *Adv. Phys.* **18** 193
[43] Lipson H S and Stokes A R 1942 The structure of graphite *Proc. R. Soc.* A **181** 101
[44] Verre R, Baranov D G, Munkhbat B, Cuadra J, Käll M and Shegai T 2019 Transition metal dichalcogenide nanodisks as high-index dielectric mie nanoresonators *Nat. Nanotechnol.* **14** 679
[45] Li Y, Chernikov A, Zhang X, Rigosi A, Hill H M, van der Zande A M, Chenet D A, Shih E-M, Hone J and Heinz T F 2014 Measurement of the optical dielectric function of monolayer transition-metal dichalcogenides: moS_2, $MoSe_2$, WS_2, and WSe_2 *Phys. Rev.* B **90** 205422
[46] Feierabend M, Morlet A, Berghauser G and Malic E 2017 Impact of strain on the optical fingerprint of monolayer transition-metal dichalcogenides *Phys. Rev.* B **96** 45425

[47] Frasco M and Chaniotakis N 2009 Semiconductor quantum dots in chemical sensors and biosensors *Sensors* **9** 7266
[48] Aas S and Bulutay C 2018 Strain dependence of photoluminescence and circular dichroism in transition metal dichalcogenides: a k • p analysis *Opt. Express* **26** 28672
[49] Roy S, Sharbirin A S, Lee Y, Bin Kim W, Kim T S, Cho K, Kang K, Jung H S and Kim J 2020 Measurement of quantum yields of monolayer TMDs using dye-dispersed PMMA thin films *Nanomaterials* **10** 1032
[50] Ruppert C, Aslan B and Heinz T F 2014 Optical properties and band gap of single- and few-layer $MoTe_2$ crystals *Nano Lett.* **14** 6231
[51] James Singh K, Ahmed T, Gautam P, Sadhu A S, Lien D-H, Chen S-C, Chueh Y-L and Kuo H-C 2021 Recent advances in two-dimensional quantum dots and their applications *Nanomaterials* **11** 1549